

Supplement to An empirical model of global climate – Part 1: A critical evaluation of volcanic cooling

T. Canty¹, N. R. Mascioli^{1,*}, M. D. Smarte^{2,**}, and R. J. Salawitch^{1,2,3}

¹ Department of Atmospheric and Oceanic Science, University of Maryland, College Park, MD

² Department of Chemistry and Biochemistry, University of Maryland, College Park, MD

³ Earth System Science Interdisciplinary Center, University of Maryland, College Park, MD

* Now at Department of Earth and Environmental Sciences, Columbia University, New York, NY

** Now at Division of Chemistry and Chemical Engineering, California Institute of Technology, Pasadena, CA

Correspondence to: T. Canty (tcanty@atmos.umd.edu)

Supplement

Section 2.2 states “As shown in Supplement, use of SOD from NOAA rather than SOD from GISS in our regression has no bearing on our finding regarding the sensitivity of $\Delta T_{\text{VOLCANO}}$ to consideration of the AMV index.” This point is illustrated in **Fig. S1**, identical to Fig. 12 of the main paper except the stratospheric optical depth (SOD) record from NOAA (Ammann et al., 2003) is used. The NOAA record of SOD is available only to the end 2008. We have extended this record to the end of 2011 by using the last available measure of SOD, 1.8×10^{-4} , for all months after December 2008, so that the regressions in **Fig. S1** cover the same time period as the regressions in Fig. 12. Comparison of the arrows on **Fig. S1**, which denote maximum SOD after the four major eruptions since 1900 (Santa María, Mount Agung, El Chichón, and Mount Pinatubo marked as SM, A, C, and P), to those on Fig. 12 reveals considerable difference between peak SOD in the NOAA record compared to the GISS record (Sato et al., 1993) after major eruptions. This difference is apparent also in Fig 2.18 of IPCC (2007), as noted in Section 2.2 of the main paper. However, maximum cooling due to Pinatubo (the absolute value of the product of C_1 and SOD $\text{MAX}_{\text{PINATUBO}}$) is quite similar for both SOD records, because the regression is most sensitive to the timing of the SOD perturbation, which is nearly identical for the two data sets. The sensitivities of $\Delta T_{\text{VOLCANO}}$ to whether the AMV index is used in the regression as well as the method used to detrend the AMV index are apparent in **Fig. S1**.

Section 3.1 states “The external forcing of global climate due to variations in the abundance of GHGs, black carbon (direct and indirect effects), TSI, stratospheric aerosols, and sulfate (direct and indirect effects) from 1900 to present are in close agreement with the representation of these terms illustrated in Fig. 1a of Hansen et al. (2005)”. **Fig. S2** shows the constraints for the RF of climate used in our simulations. This figure is designed to be directly comparable to Fig. 1a of Hansen et al. (2005) and is included here to assure readers our model constraints are consistent with values commonly used in other studies.

Section 3.2.2 states “in the Supplement, we show simulations for different time series of NAA RF_i , all having $\text{NAA RF}_{2005} = -1.0 \text{ W m}^{-2}$, based on values of α_{COOL} and α_{HEAT} at the intersection of the red line and the “High Road”, “Middle Road”, and “Low Road” of Fig. 4.” **Figure S3** illustrates this point. Regressions in **Fig. S3** are all related to Fig. 6d, a regression of the CRU4 global temperature anomaly found using $\text{AMV}_{\text{Had3 AF}}$. In the main paper, we used

values of the scaling parameters, α_{COOL} and α_{HEAT} , for $\text{NAA RF}_{2005} = -1.0 \text{ W m}^{-2}$ along the “Middle Road” of Fig. 4. All regressions shown in **Fig. S3** use $\text{NAA RF}_{2005} = -1.0 \text{ W m}^{-2}$ as well as $\text{AMV}_{\text{Had3 AF}}$. Panel *a* of **Fig. S3** uses values of α_{COOL} and α_{HEAT} along the “Low Road” of Fig. 4; panel *b* is for values of these parameters along the “Middle Road”, and panel *c* is for values along the “High Road”. The nearly identical appearance of these regressions supports our contention that the important factor for our analysis is the value of NAA RF_{2005} , rather than the specific combination of α_{COOL} and α_{HEAT} used to arrive at NAA RF_{2005} . We have conducted extensive testing of these scaling parameters and the central importance of NAA RF_{2005} is robust. As described in the main paper, year 2005 was chosen as the benchmark because of the focus within IPCC (2007) on estimating NAA RF for 2005. Our entire analysis hardly differs if we had used 2011 as the benchmark. Better definition of the uncertainty in net anthropogenic aerosol radiative forcing for the contemporary atmosphere (2005 or 2011) is vital for reducing uncertainties inherent in global warming projections (Mascioli et al., 2012). The determination of $\Delta T_{\text{VOLCANO}}$ is moderately sensitive to uncertainty in NAA RF_{2005} (or NAA RF_{2011}), but the effect on $\Delta T_{\text{VOLCANO}}$ due to inclusion of the AMV index in the regression model is found for all values of NAA RF_{2005} .

Section 3.2.3 states “in Supplement, we show that our overall conclusions are unaffected if KaplanSST2 is used”. This point is illustrated by **Fig. S4**, identical to Fig. 12 except the SST record from KaplanSST2 has been used for the definition of the AMV index. **Fig. S4** is extremely similar to Fig. 12 in the main paper, demonstrating the insensitivity of our scientific conclusions to which SST record is used.

Section 4.1 states “Further support for the validity of the use of the AMV index, as a proxy for the effect of variations in the strength of the AMOC on climate, are provided by an analysis that examines the CRU4 temperature record in each hemisphere (see Supplement).” **Fig. S5** shows regressions for each hemisphere. The influence of the AMV index is much stronger on the Northern Hemisphere (NH) temperature record. The value of χ^2 drops from 1.35 for the regression that does not consider the AMV index (**Fig S5a**) to 0.52 when this index is added (**Fig S5b**). **Figs. S5a** and **S5b** show many features of the NH temperature record, such as pre-WWI cooling, post WWI heating, as well as the temperature rise from 1990 to present are simulated much better by the MLR model when the AMV index is included. Cooling in the NH attributed to Pinatubo falls from 0.49°C (**Fig. S5a**) to 0.23°C (**Fig. S5b**) when the AMV index is added to the regression. The influence of the AMV index is much smaller for the Southern Hemisphere (SH), as reflected by a smaller value of C_4 (AMV regression coefficient) and little effect on χ^2 when this index is introduced (**Fig. S5c** and **S5d**). The influence of variations in the strength of the AMOC is considerable stronger than ENSO for the NH temperature record, whereas ENSO is much stronger than AMOC for the SH. These behaviors are consistent with expectation for both hemispheres.

Section 4.1.2 states “The power spectrum of the AMV index is shown in Supplement”. **Fig. S6** shows the normalized power spectrum (maximum power set to unity) of the $\text{AMV}_{\text{Had3 AF}}$ index time series shown in Fig. 5d. Maximum power occurs for frequencies lower than about 55 yr^{-1} . As emphasized in the main text, our scientific conclusions do not depend on whether or not North Atlantic SSTs, upon which the $\text{AMV}_{\text{Had3 AF}}$ index is based, vary in a purely periodic fashion.

Section 4.1.2 also states “If indices for ENSO and SOD are used in the model, rather than T_{ENSO} and T_{VOLCANO} , values of 0.12 and 0.18°C are found for $\Delta T_{\text{PINATUBO}}$ for the 1/9 yr⁻¹ and 1/73 yr⁻¹ filters, respectively.” These model results are shown in **Figs. S7a** and **S7b**. Whether we use the thermodynamic response approach (i.e., Fig. 7 of main) or the index approach (**Fig S7**) for ENSO and volcanoes, we find the importance of the AMV index is dominated by the low frequency, high amplitude component of this proxy for variations in the strength of the AMOC. Given the 2 to 3 year e-folding time for the disappearance of stratospheric sulfate following major volcanic eruptions (e.g., Ammann et al., 2003), these figures provide strong scientific evidence that the primary finding of our study is not compromised by mis-attribution of volcanic cooling due to a putative rapid decline of North Atlantic SST following major volcanic eruptions.

Section 4.3 states “as shown in the Supplement, the derivative of OHC from Church et al. (2011), an update to the record of Domingues et al. (2008), bears no relation to SOD (hence, the conclusion of Murphy et al. (2009) seems highly dependent on which OHC record is used, and possibly how the data are smoothed)” as well as “also, there is no suggestion that when SOD achieves a local maximum (i.e. peak volcanic perturbation), the AMV index is at a local minimum either coincident in time with peak SOD (as suggested by the GCM of Booth et al., 2012) or ~2 to 3 yr after peak SOD (as suggested by the GCM studies of Stenchikov et al., 2009 and Zanchettin et al., 2012) (see Supplement).” **Figure S8** shows the GISS time series of SOD (panel *a*), the time derivative of Ocean Heat Content (OHC) data from Church et al. (2011) which equals OHE (e.g., Murphy et al., 2009) (panel *b*), and a scatter plot of these two physical quantities (panel *c*). For the scatter plot, we relate SOD to the value of OHE six months into the future, to represent the adjustment time of the stratosphere to the RF perturbation induced by the volcano. Enhanced values of SOD associated with the eruptions of Agung, El Chichón, and Pinatubo as well as OHE (6 month delay) are color coded using the same palette as Fig. 10. This is no significant relation between SOD and OHE. The conclusion of no relation between SOD and OHE holds for 0 time shift, a time shift of 1 year, or any other time shift. Certainly there are valleys in OHE that could plausibly be related to SOD, such as the dip around 1968 that could be related to Agung. However, the OHE record shown in **Fig. S8** exhibits 6 well defined, decadal time scale valleys, between 1950 and 2010. In contrast, the SOD record exhibits only 3 strong peaks during this same period of time.

Murphy et al. (2009) describe a visual relation between OHE and SOD, where OHE was found after applying an 8 year linear fit smoothing to the OHC data of Domingues et al. (2008). We have computed OHE using running means of 3, 5, 7, and 9 years applied to the OHC data of Church et al. (2011) and we still find no significant relation between OHE and SOD. Murphy et al. (2009) do not justify use of “8 year linear fit smoothing” to the OHC record.

Measurements of OHC vary over time, either due to noise in the estimate or perhaps the stochastic nature of atmosphere to ocean heat transfer when examined on a yearly basis. Regardless, the data records we have examined show no evidence for volcanic influence on ocean circulation, despite the indication for such an influence from several independent GCM studies (Stenchikov et al., 2009; Booth et al., 2012; Zanchettin et al., 2012).

Section 4.3 also states “as shown in Supplement, this plot looks similar for $\text{AMV}_{\text{Had3 SST}}$ and $\text{AMV}_{\text{Had3 Lin}}$, except the AMV index is much closer to neutral after the eruption of Santa Maria

when detrended using global SST”. **Figures S9** and **S10** are identical to Fig. 10 expect $AMV_{Had3\ SST}$ (**Fig. S9**) and $AMV_{Had3\ Lin}$ (**Fig. S10**) are used rather than $AMV_{Had3\ AF}$. The subscripts SST, LIN, and AF refer to various ways of detrending the AMV index, as described in Section 3.2.3. All of the AMV indices are based on North Atlantic SSTs (HadSST3) from the Hadley Center (Kennedy et al., 2011a,b), denoted by use of Had3 in the subscript. Together **Fig. S9**, **Fig. S10**, and Fig. 10 of main can be used to make two important points: 1) when SOD was enhanced following the four major eruptions since 1900, as well as 6 months before each eruption, the AMV index tended to be more negative than positive regardless of how this index is detrended; 2) the value of the AMV index in the early 20th century is most sensitive to how detrending is conducted. Smaller values of $\Delta T_{VOLCANO}$ are found using $AMV_{Had3\ Lin}$ or $AMV_{Had3\ AF}$, compared to $AMV_{Had3\ SST}$, due to the sensitivity of the regression coefficients to the value of the AMV index after the eruption of Santa Maria in October 1902. As discussed in the main paper, observed cooling during the pre-WWI time period and warming during the WWII time period is modeled better using $AMV_{Had3\ Lin}$ or $AMV_{Had3\ AF}$ than $AMV_{Had3\ SST}$, supporting the possibility these representations of the AMV are valid for the early 20th century.

Section 5.1 of the paper states “Nearly all of this perturbation occurs in the tropics: the net radiative effect of Pinatubo poleward of 20° latitude was small in the Northern Hemisphere and essentially zero in the Southern Hemisphere (see Supplement).” **Figure S11** shows the perturbation to SW, LW, and Net (LW–SW) radiation at the top of the atmosphere measured by ERBE. There is no discernable change in the Net budget, following the eruption of Pinatubo, poleward of 20°S. The SW and LW components each show an effect, but the changes in these components are balanced. As noted in the main paper, the treatment of the stratospheric response of this anomaly (the LW perturbation is due to absorption of thermal radiation within the stratosphere by volcanic aerosols, and re-radiation in all directions) and the downward influence is critical. The perturbations to SW and LW are more distinct in the Northern Hemisphere extra-tropics, but the Net perturbation is hard to distinguish from the noise in the climate system (i.e., without the gray shading or knowledge of when Pinatubo erupted, volcanic influence on the Net budget would be hard to discern).

The main paper states “the formulation of χ^2 is based on annual temperature anomalies, rather than monthly anomalies, because the monthly observed temperature anomaly exhibits an autocorrelation that differs significantly from that of modeled temperature whereas the CRU4 annual temperature anomaly displays an autocorrelation that closely resembles modeled temperature”. **Figure S12** shows autocorrelations of modeled and measured temperature anomalies, for monthly time series (panel a) and annual time series (panel b). The difference in the autocorrelation of the measured and modeled temperature anomaly on a monthly time grid indicates either persistence in the measurement due to some type of instrumental averaging, in which case the degrees of freedom used in the denominator of the expression for χ^2 (Eq. 7) would have to be reduced, or else the presence of a process that affects global temperature on monthly time scales that is not represented in the model. The close match between the autocorrelation of the measured and modeled anomaly on an annual time grid suggests the use of N_{YEARS} in the denominator of Eq. (7): i.e., the auto-regressive behavior of annual mean temperature is well simulated by the model.

Finally, the main paper states “as shown in Supplement, regressions that account for the effect of variations in the strength of the AMOC on climate give a remarkably accurate description of $\Delta\bar{T}_{\text{OBS}}$ from 1900 to present for NAA RF₂₀₀₅ ranging from -1.6 W m^{-2} to -0.4 W m^{-2} , provided the climate feedback parameter (λ) is allowed to adjust such that the cost function is minimised.” This point is illustrated in **Figure S13**, which shows time series of $\Delta\bar{T}_{\text{OBS}}$ and $\Delta\bar{T}_{\text{MDL}}$, the observed and modeled annual mean global temperature anomalies, from 1900 to the end of 2011. The gray shading denotes $2 \times \bar{\sigma}_{\text{OBS}}$, the uncertainty of the annual global mean temperature provided by the Hadley Centre (Morice et al., 2012). We use the upper and lower 95% uncertainty limits given in columns 11 and 12 of file HadCRUT4.4.1.0.annual_ns_avg.txt last accessed April 7, 2013. The values of the climate feedback parameter associated with each regression as well as χ^2 are indicated. The best fit regression provides a remarkably accurate depiction of the observed annual temperature anomaly. Almost without exception the model lies within the 2σ range of measurement uncertainty, due to the cantilevering of NAA RF2005 and λ (Mascioli et al., 2012).

References

- Ammann, C. M., G. A. Meehl, W. M. Washington, and C. S. Zender, A monthly and latitudinally varying volcanic forcing dataset in simulations of 20th century climate, *Geophys. Res. Lett.*, 30, 1657, doi:10.1029/2003GL016875, 2003.
- Booth, B. B. B., Dunstone, N. J., Halloran, P. R., Andrews, T., and Bellouin, N.: Aerosols implicated as a prime driver of twentieth-century North Atlantic climate variability, *Nature*, 484, 228–232, doi:10.1038/nature10946, 2012.
- Church, J. A., White, N. J., Konikow, L. F., Domingues, C. M., Cogley, J. G., Rignot, E., Gregory, J. M., van den Broeke, M. R., Monaghan, A. J., and Velicogna, I.: Revisiting the Earth's sea-level and energy budgets from 1961 to 2008, *Geophys. Res. Lett.*, 38, L18601, doi:10.1029/2011GL048794, 2011.
- Domingues, C. M., Church, J. A., White, N. J., Glecker, P. J., Wijffels, S. E., Barker, P. M., and Dunn, J. R.: Improved estimates of upper-ocean warming and multidecadal sea-level rise, *Nature*, 453, 1090–1093, doi:10.1038/nature07080, 2008.
- Hansen, J., Nazarenko, L., Ruedy, R., Sato, M., Willis, J., Del Genio, A., Koch, D., Lacis, A., Lo, K., Menon, S., Novakov, T., Perlwitz, J., Russell, G., Schmidt, G. A., and Tausnev, N.: Earth's energy imbalance: confirmation and implications, *Science*, 309, 1431–1435, doi:10.1126/science.1110252, 2005.
- IPCC, 2007: *Climate Change 2007: The Physical Science Basis*. Contribution of Working Group I to the Fourth Assessment Report of the Intergovernmental Panel on Climate Change [Solomon, S., Qin, D., Manning, M., Chen, Z., Marquis, M., Averyt, K. B., Tignor, M., and Miller, H. L. (eds.)], Cambridge University Press, Cambridge, United Kingdom and New York, NY, USA, 996 pp., 2007.
- Kennedy J. J., Rayner, N. A., Smith, R. O., Saunby, M. and Parker, D. E.: Reassessing biases and other uncertainties in sea-surface temperature observations since 1850 part 1: measurement and sampling errors, *J. Geophys. Res.*, 116, D14103, doi:10.1029/2010JD015218, 2011a.
- Kennedy J. J., Rayner, N. A., Smith, R. O., Saunby, M. and Parker, D. E.: Reassessing biases and other uncertainties in sea-surface temperature observations since 1850 part 2: biases and homogenization, *J. Geophys. Res.*, 116, D14104, doi:10.1029/2010JD015220, 2011b.
- Mascioli, N. R., Canty, T., and Salawitch, R. J.: An empirical model of global climate – Part 2: Implications for future temperature, *Atmos. Chem. Phys. Discuss.*, 12, 23913–23974, doi:10.5194/acpd-12-23913-2012, 2012.
- Morice, C. P., Kennedy, J. J., Rayner, N. A., and Jones, P. D.: Quantifying uncertainties in global and regional temperature change using an ensemble of observational estimates: the HadCRUT4 data set, *J. Geophys. Res.*, 117, D08101, doi:10.1029/2011JD017187, 2012.
- Murphy, D. M., Solomon, S., Portmann, R. W., Rosenlof, K. H., Forster, P. M., and Wong, T.: An observationally based energy balance for the Earth since 1950, *J. Geophys. Res.*, 114, D17107, doi:10.1029/2009JD012105, 2009.
- Sato, M., Hansen, J. E., McCormick, M. P., and Pollack, J. B.: Stratospheric aerosol optical depths, 1850–1990. *J. Geophys. Res.*, 98, 22987–22994, doi:10.1029/93JD02553, 1993.
- Stenchikov, G., Delworth, T. L., Ramaswamy, V., Stouffer, R. J., Wittenberg, A., and Zeng, F.: Volcanic signals in oceans, *J. Geophys. Res.*, 114, D16104, doi:10.1029/2008JD011673, 2009.
- Zanchettin, D., Timmreck, C., Graf, H.-F., Rubino, A., Lorenz, S., Lohmann, K., Kruger, L., Jungclaus, J. H.: Bi-decadal variability excited in the coupled ocean-atmosphere system by strong tropical volcanic eruptions, *Clim. Dyn.*, 39, 419–444, doi:10.1007/s00382-011-1167-1, 2012.

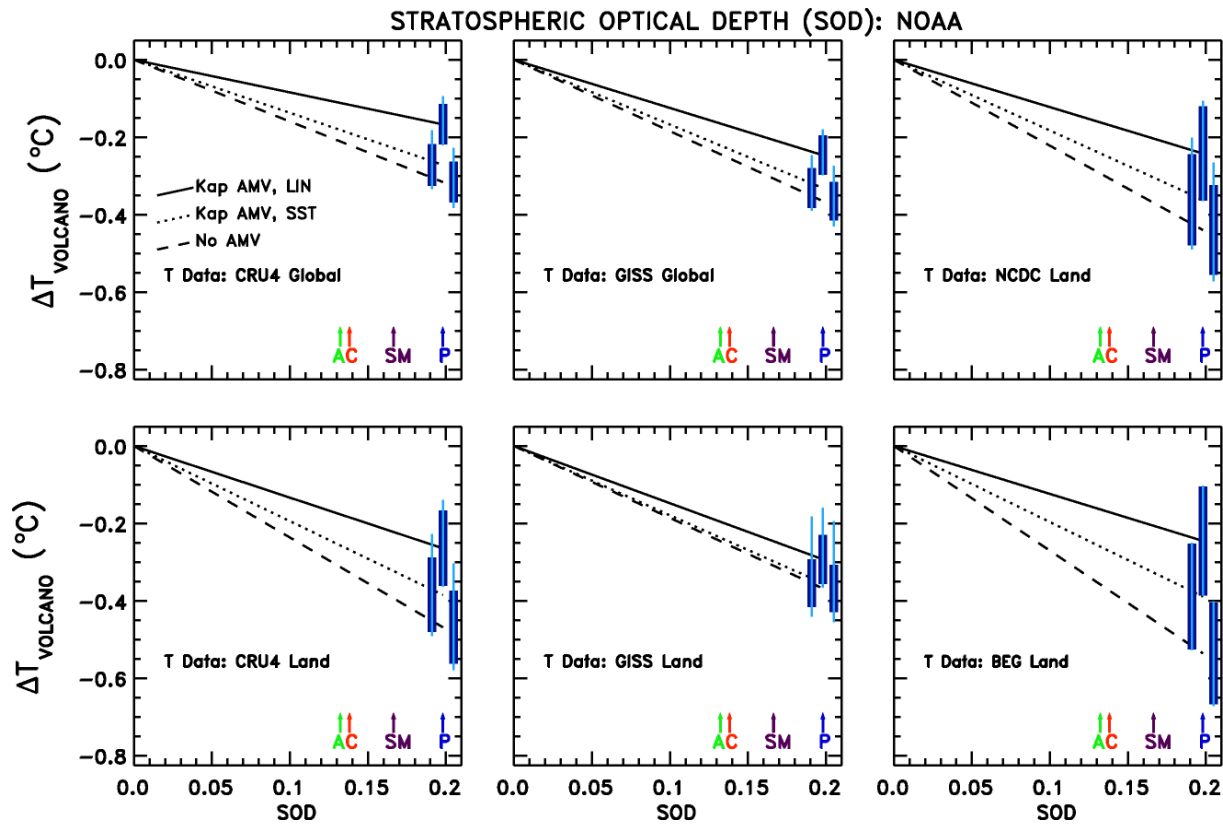


Fig. S1. Same as Fig. 12 in the main paper, except the NOAA record of SOD from Amman et al. (2003) is used.

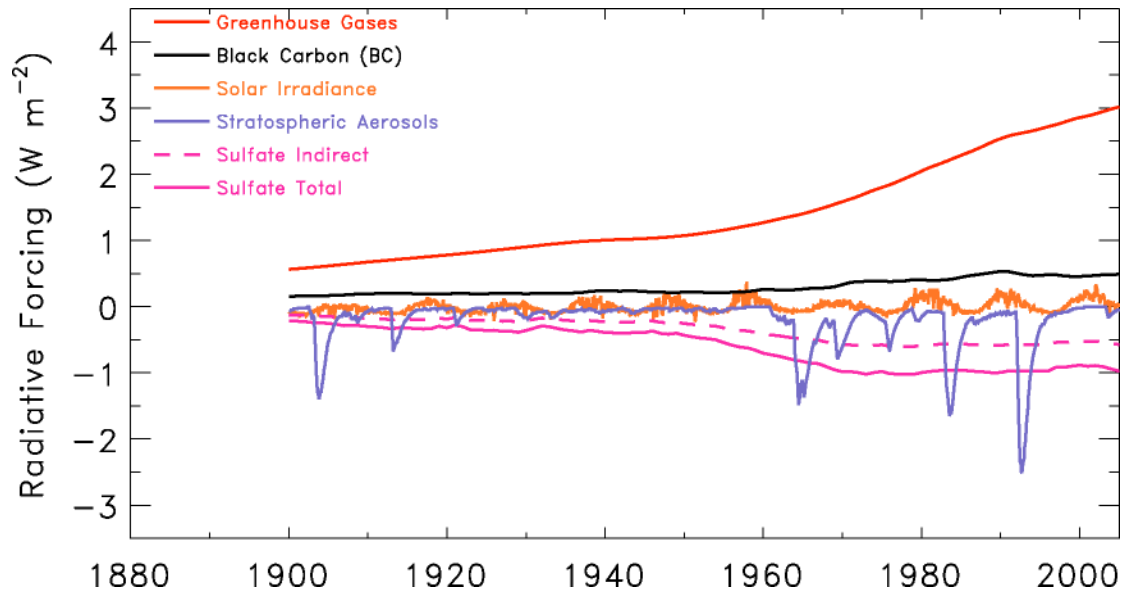


Fig. S2. External constraints for the change of RF at the tropopause, for the MLR simulations of the main paper, due to the sum of all GHGs, the total RF due to black carbon, solar irradiance, stratospheric aerosols (i.e., volcanoes), the indirect effect of RF due to sulfate aerosols, and the total RF due to sulfate aerosols (as indicated). The RF due to stratospheric aerosols is based on scaling 0.15, the maximum value of optical depth of the NOAA SOD index after the eruption of Mt. Pinatubo, to -2.51 W m^{-2} , the maximum value of Net radiative anomaly measured by ERBE between 60°S and 60°N following this eruption (Fig. 15).

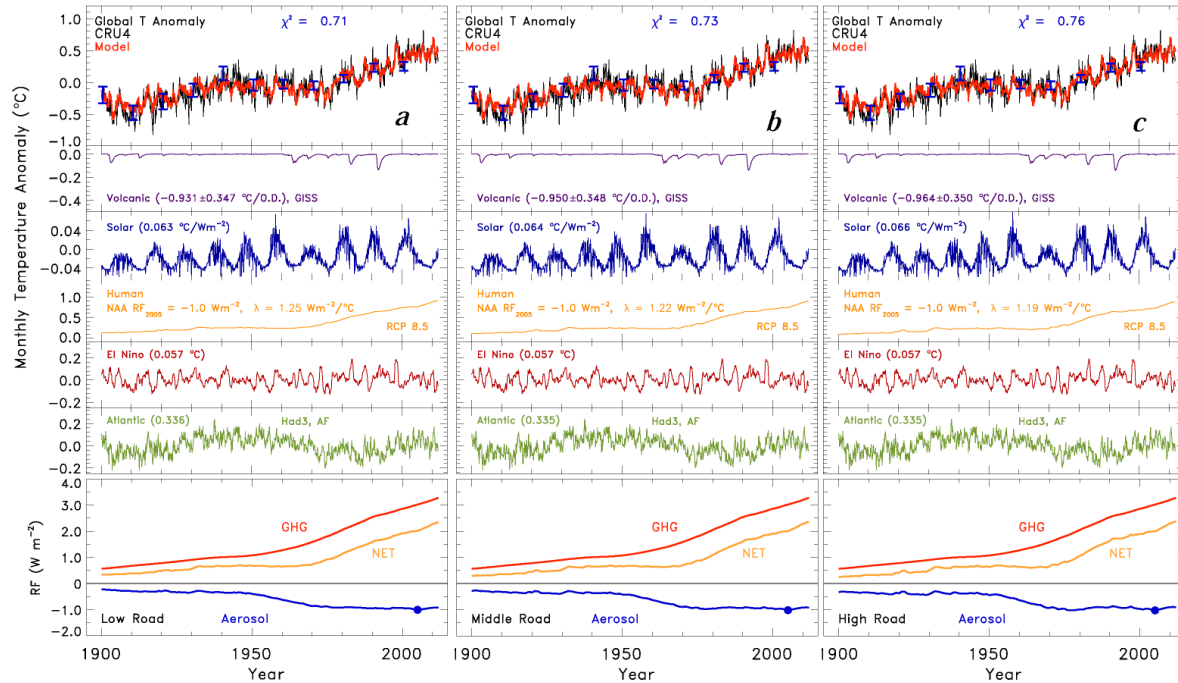


Fig. S3. Same as Fig. 6d in the main paper except rungs of the ladder plots for PDO and IOD are not shown, because these terms are small, and a panel has been added (lowest rung) showing time series of NAA RF, GHG RF, and the net anthropogenic RF of climate (termed AF in the main paper). **(a)** Regression using $\text{NAA RF}_{2005} = -1.0 \text{ W m}^{-2}$ for values of α_{COOL} and α_{HEAT} along the “Low Road” of Fig. 4. **(b)** Regression using $\text{NAA RF}_{2005} = -1.0 \text{ W m}^{-2}$ for values of α_{COOL} and α_{HEAT} along the “Middle Road” of Fig. 4 (this regression is identical to that shown in Fig. 6d of the main paper). **(c)** Regression using $\text{NAA RF}_{2005} = -1.0 \text{ W m}^{-2}$ for values of α_{COOL} and α_{HEAT} along the “High Road” of Fig. 4. All regressions use $\text{AMV}_{\text{Had3 AF}}$ (see main text).

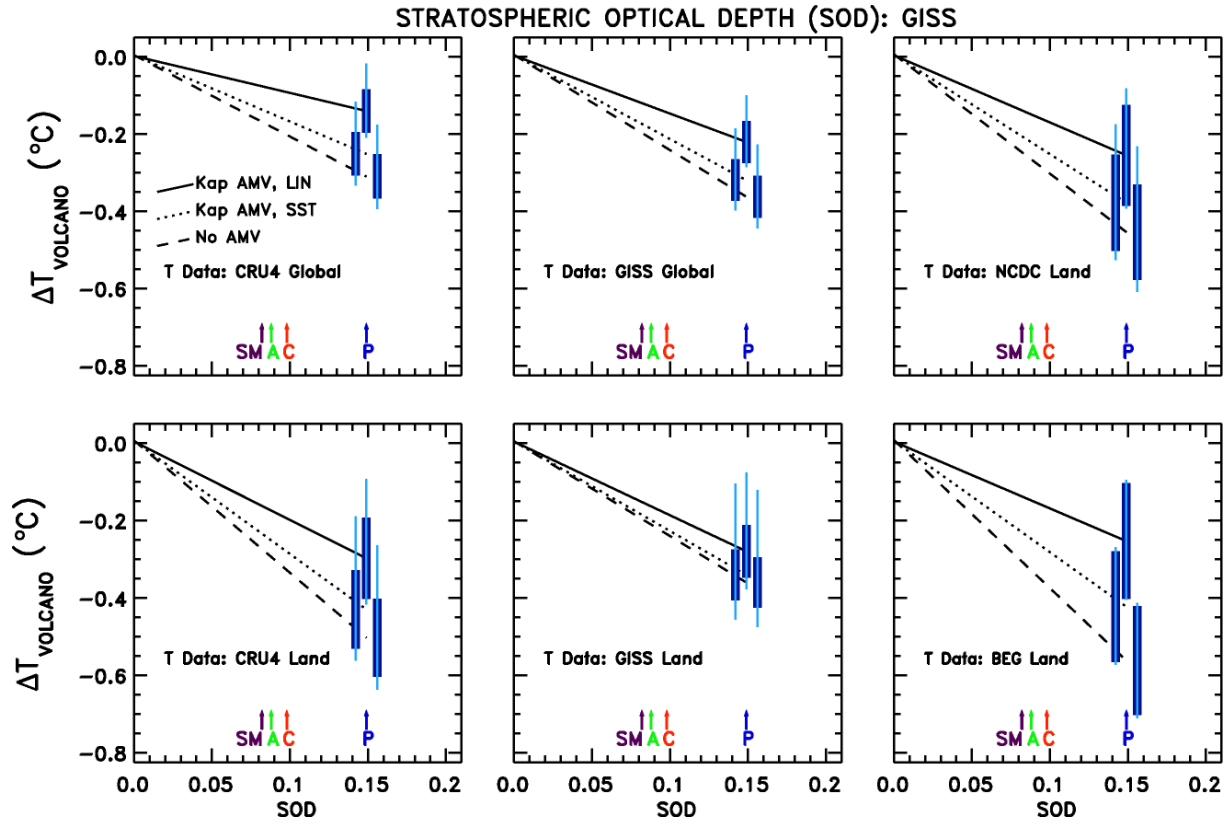


Fig. S4. Same as Fig. 12 in the main paper, except the Kaplan Extended SST V2 record from NOAA (Kaplan et al., 1998; Enfield et al., 2001; see also Appendix B) has replaced HadSST3 for the definition of the AMV index.

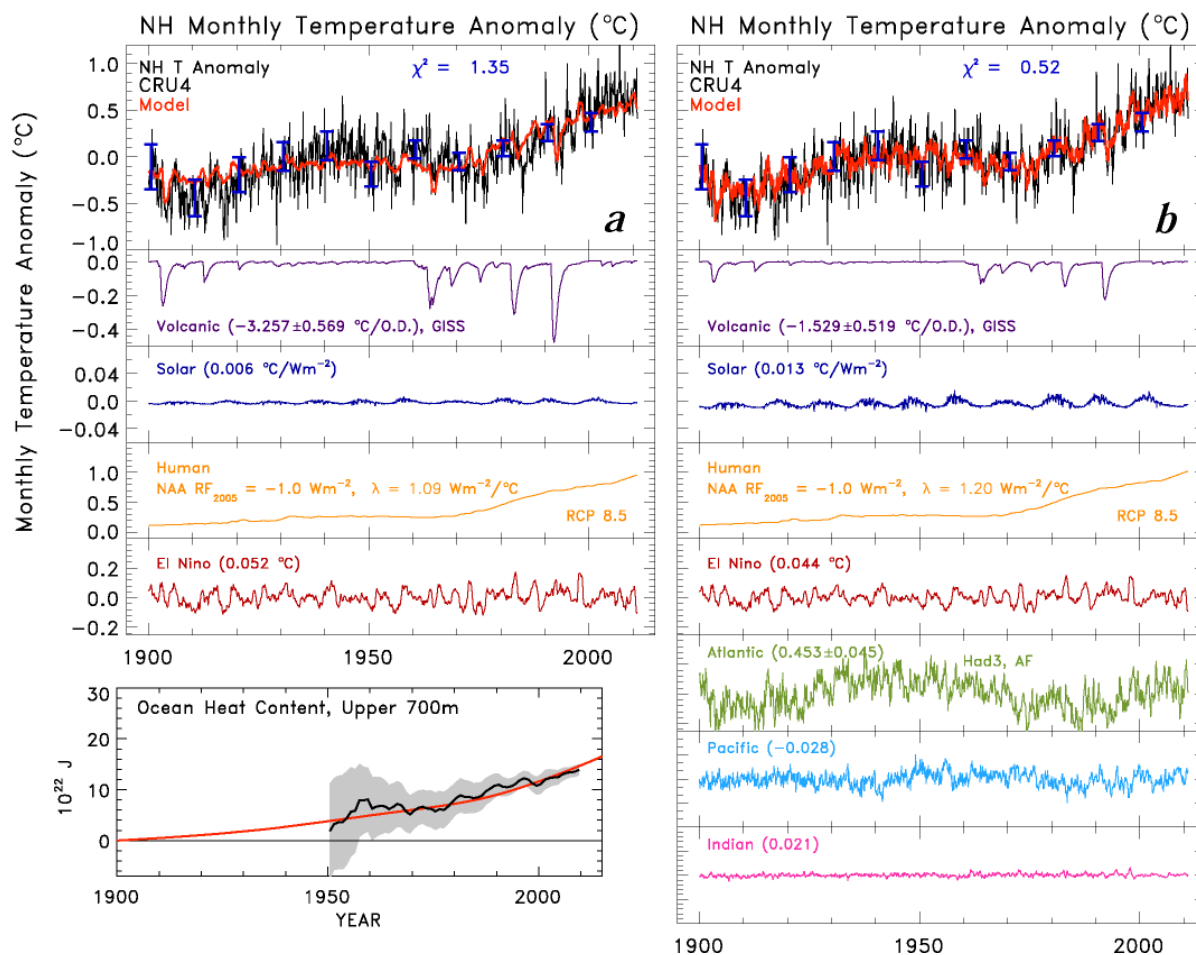


Fig. S5. (a) and (b). Same as Fig. 6a and 6d in the main paper, except CRU4 data for the Northern Hemisphere are used. The value of OHE that governs Q_{OCEAN} (i.e., numerical value entered into Eq. (5) and data shown in the Ocean Heat Content panel) has been reduced by a factor 2 to reflect the hemispheric nature of the regression.

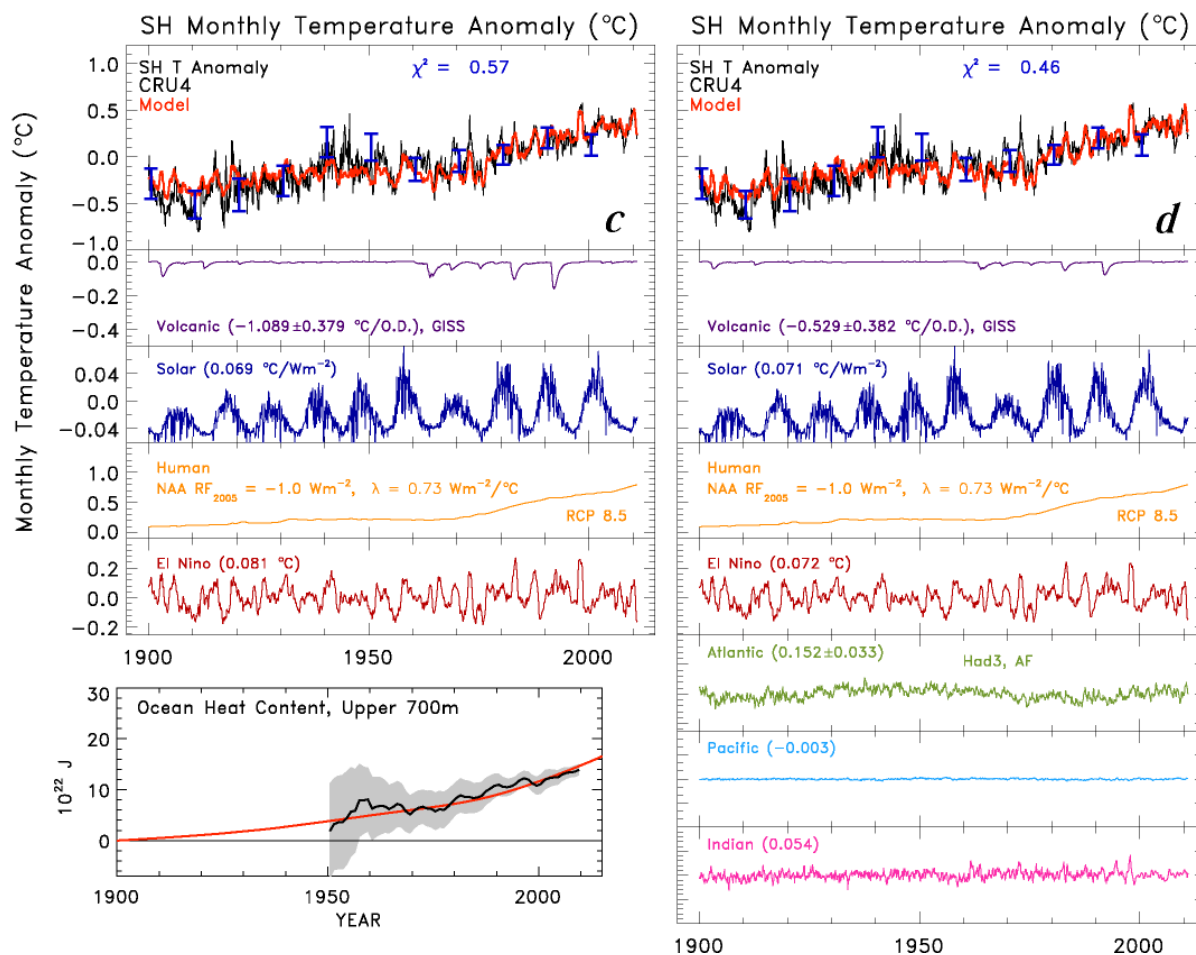


Fig. S5. (c) and (d). Same as Fig. 6a and 6d in the main paper, except CRU4 data for the Southern Hemisphere are used. The value of OHE that governs Q_{OCEAN} (i.e., numerical value entered into Eq. (5) and data shown in the Ocean Heat Content panel) has been reduced by a factor 2 to reflect the hemispheric nature of the regression.

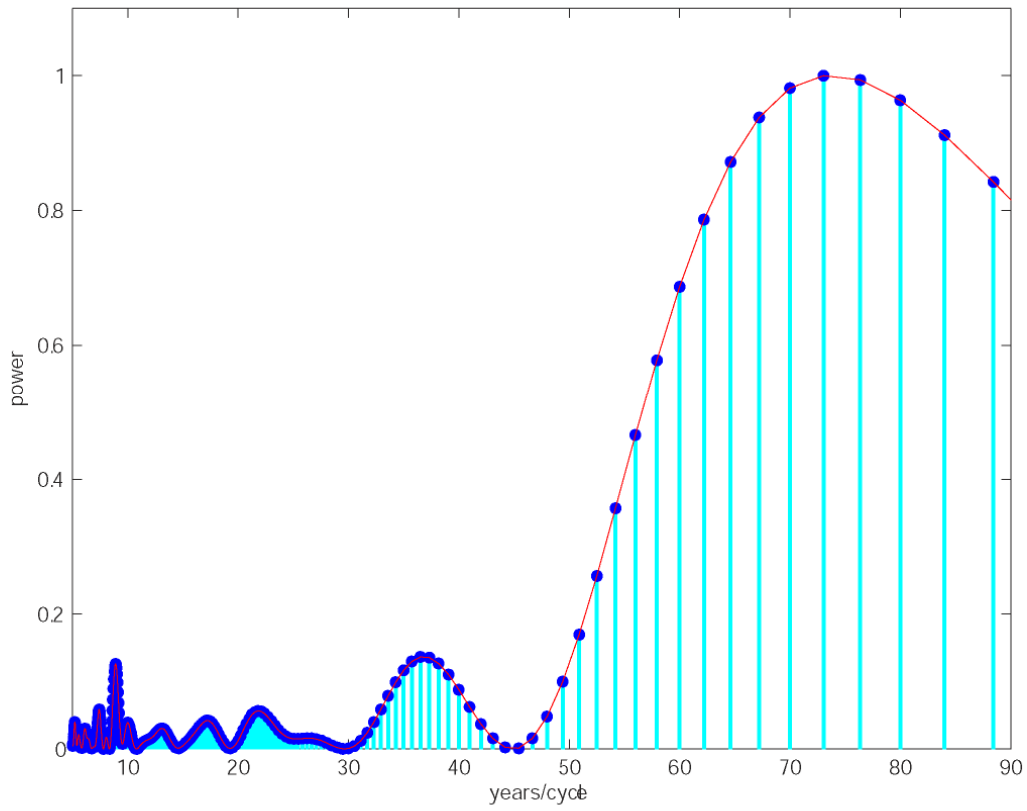


Fig. S6. Power spectrum of the AMV index detrended using Anthropogenic RF of climate (i.e., time series shown in Fig. 5d).

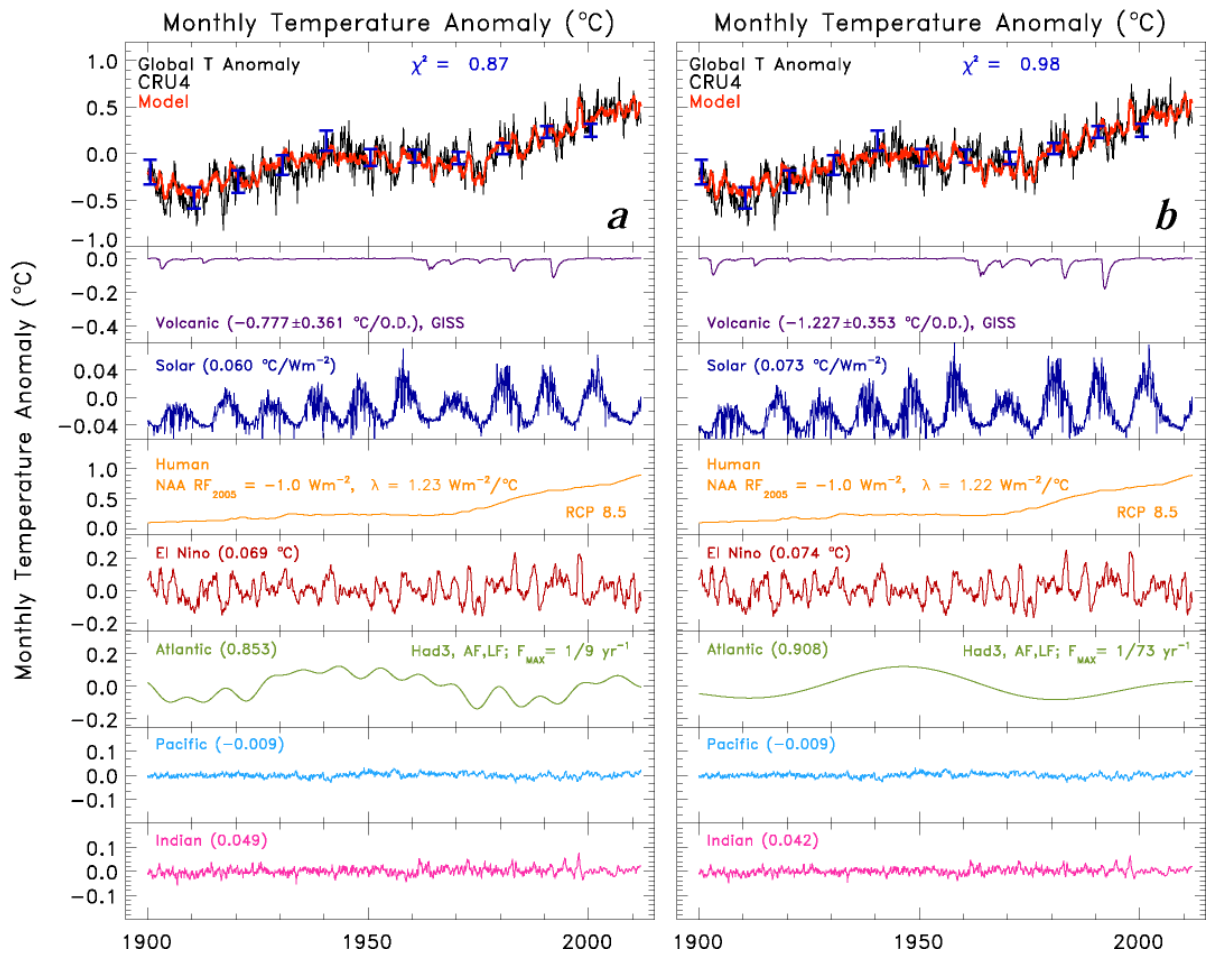


Fig. S7. Same as Fig 6d except the AMV index has been filtered to remove components with frequencies higher than $1/9$ yr⁻¹ [panel (a)] and higher than $1/73$ yr⁻¹ [panel (b)].

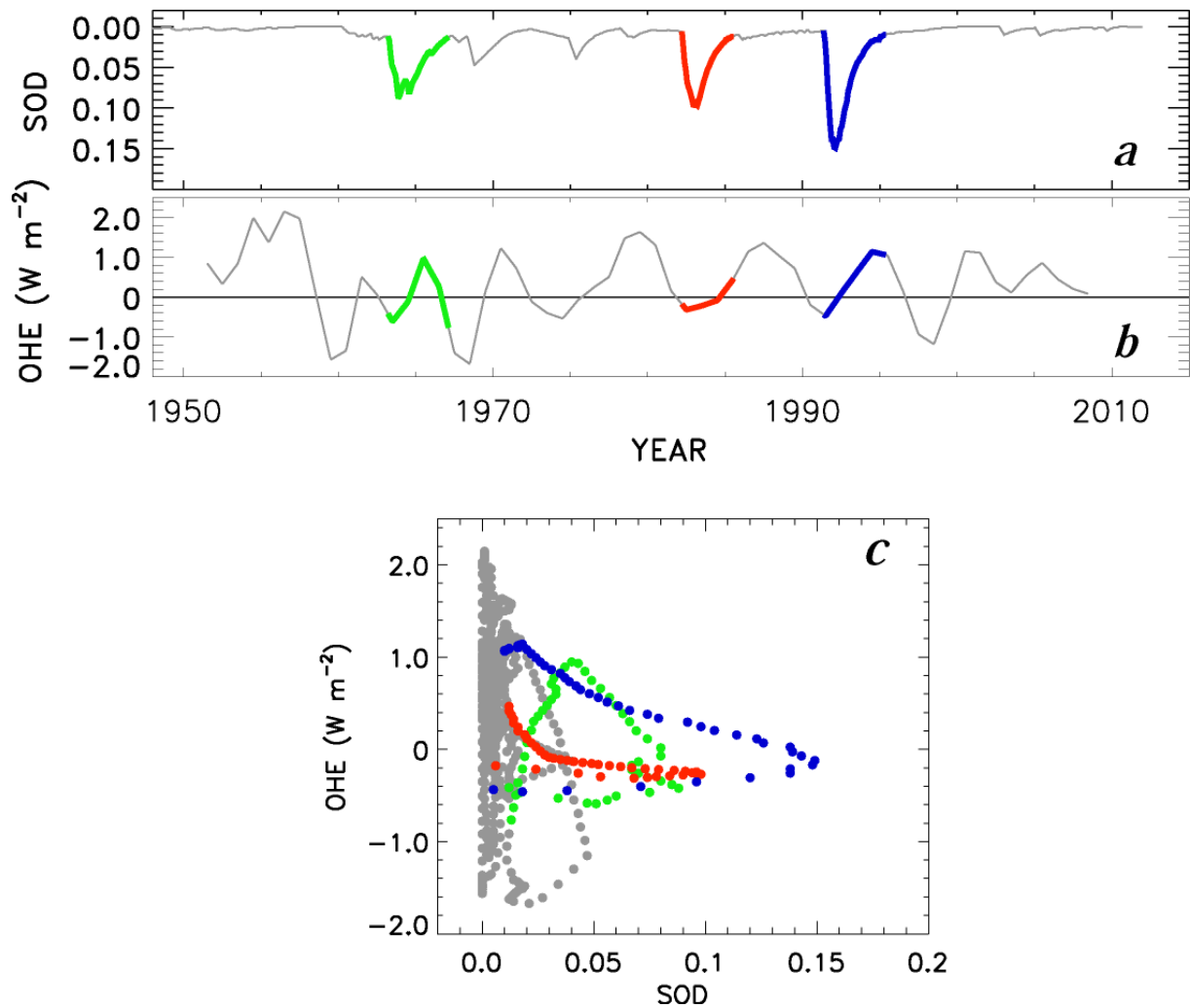


Fig. S8. (a) Monthly mean stratospheric optical depth (SOD) from Sato et al. (1993). The three major volcanoes since 1950, Mount Agung (green), El Chichón (red), and Mount Pinatubo (blue) are indicated. **(b)** Ocean Heat Export (OHE) found by taking the derivative with respect to time of the Ocean Heat Content (OHC) record of Church et al. (2011). OHC is provided on an annual basis.

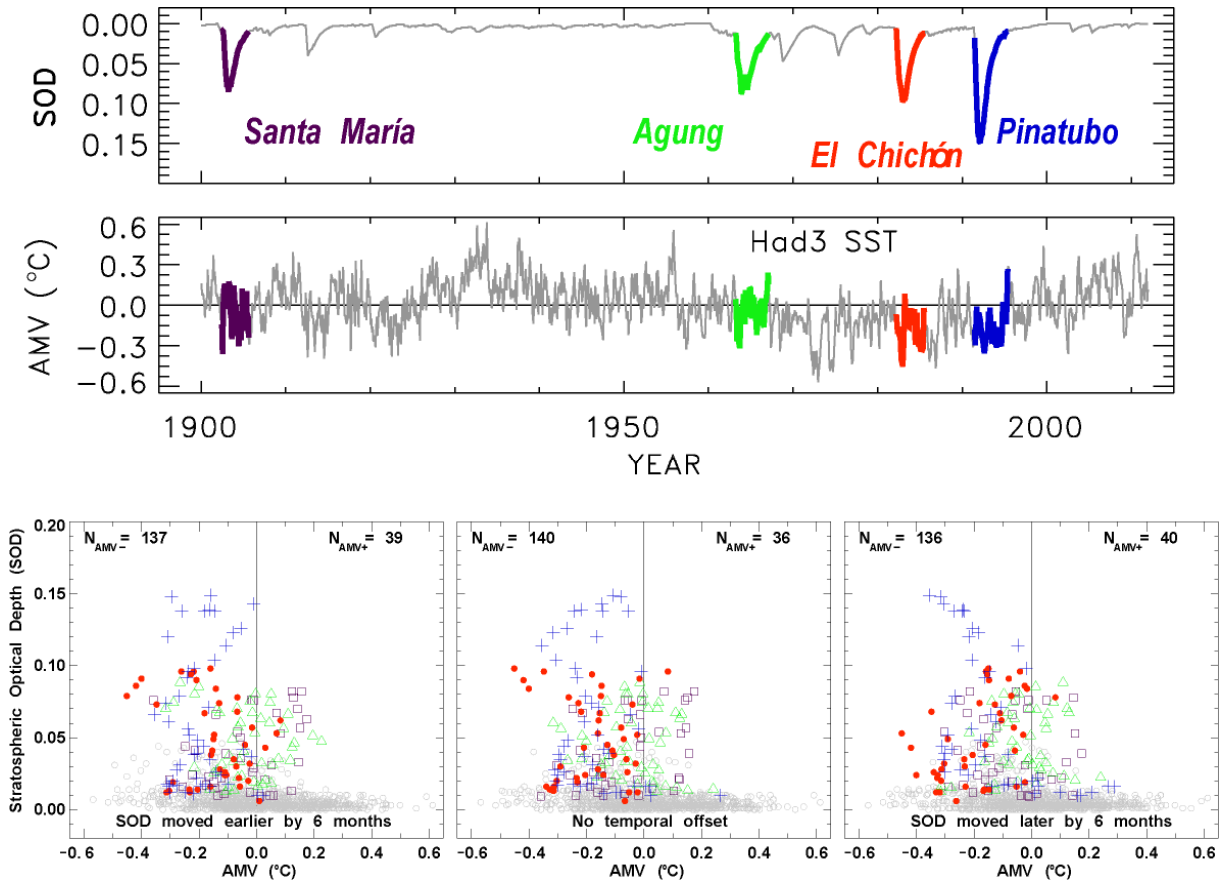


Fig. S9. Same as Fig. 10 except $AMV_{Had3\ SST}$ is used, rather than $AMV_{Had3\ AF}$.

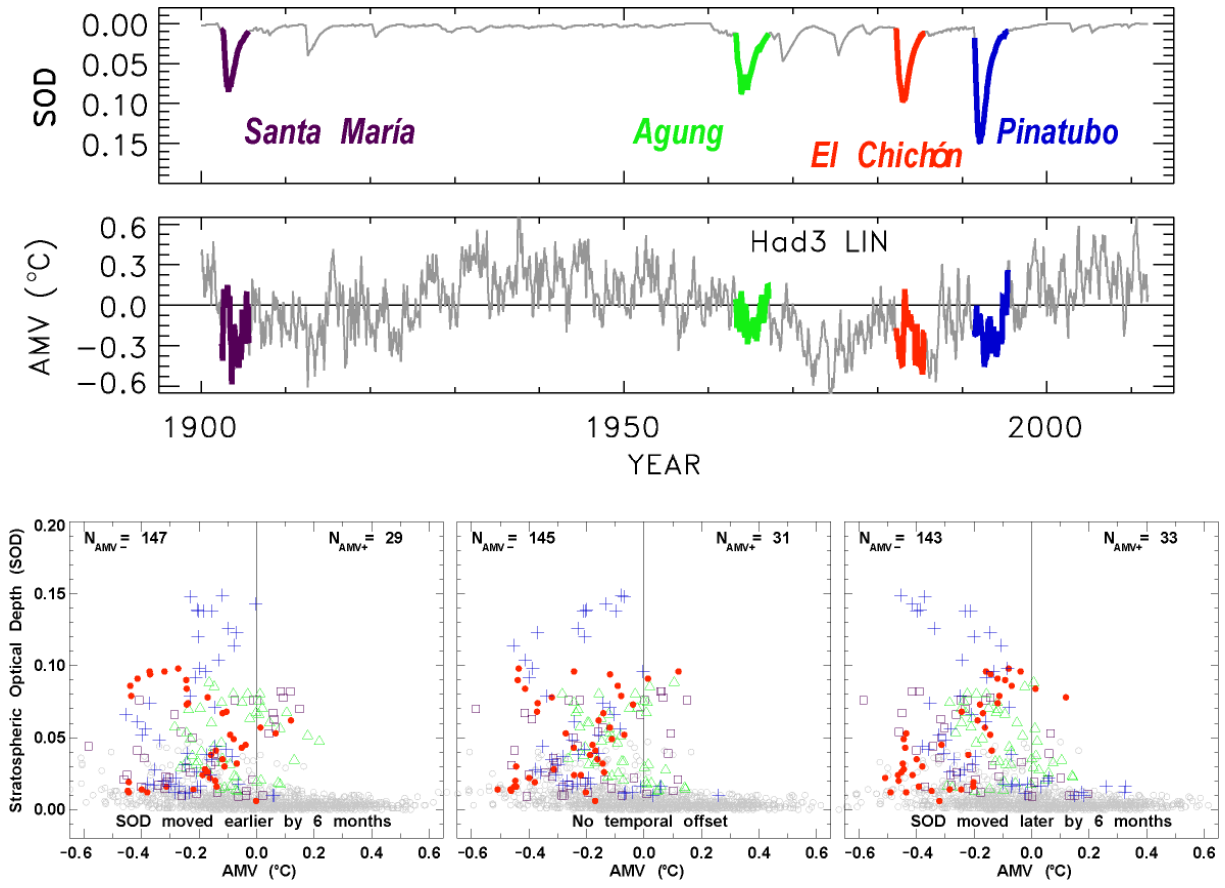


Fig. S10. Same as Fig. 10 except $AMV_{Had3\ LIN}$ is used, rather than $AMV_{Had3\ AF}$.

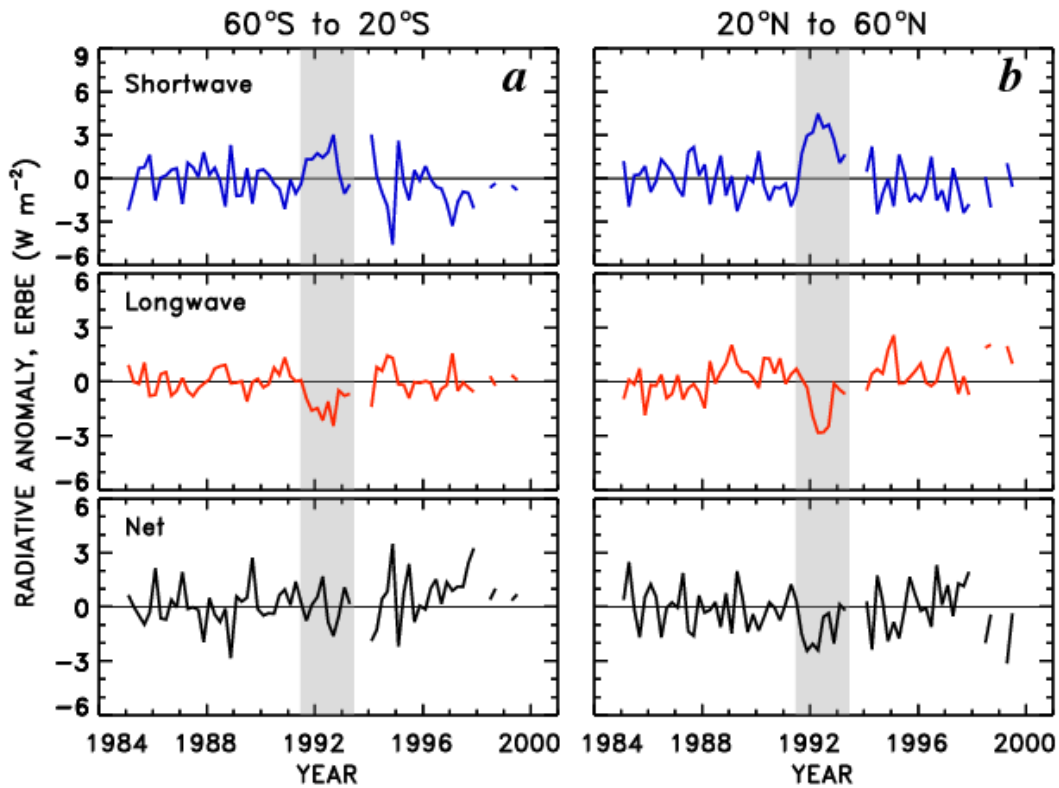


Fig. S11. Same as Fig. 15 except for the 60°S to 20°S and 20°N to 60°N latitude regions. Analysis based on raw data provided as 72-day means.

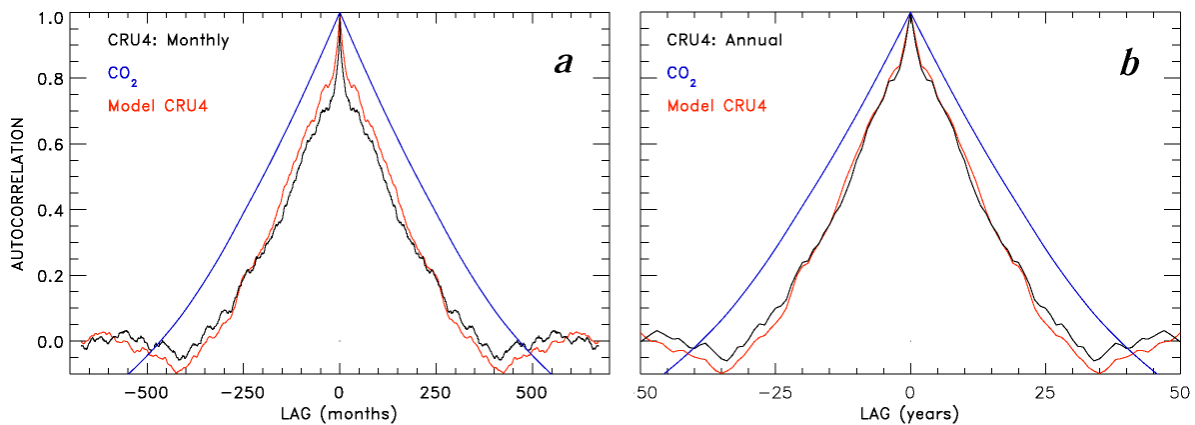


Fig. S12. Panel (a) Autocorrelation of $\Delta T_{\text{OBS } i}$ (blue) and $\Delta T_{\text{MDL } i}$ (red) as a function of the number of lagged months, from a simulation of temperature from 1900 to end of 2011 on a monthly time grid. The autocorrelation of annually averaged CO₂ from RCP 8.5 sampled on a monthly basis is also shown. Panel (b) Same as (a), except for $\overline{\Delta T}_{\text{OBS } j}$ and $\overline{\Delta T}_{\text{MDL } j}$, the annually averaged global temperature anomaly computed following post processing of the monthly regression and data.

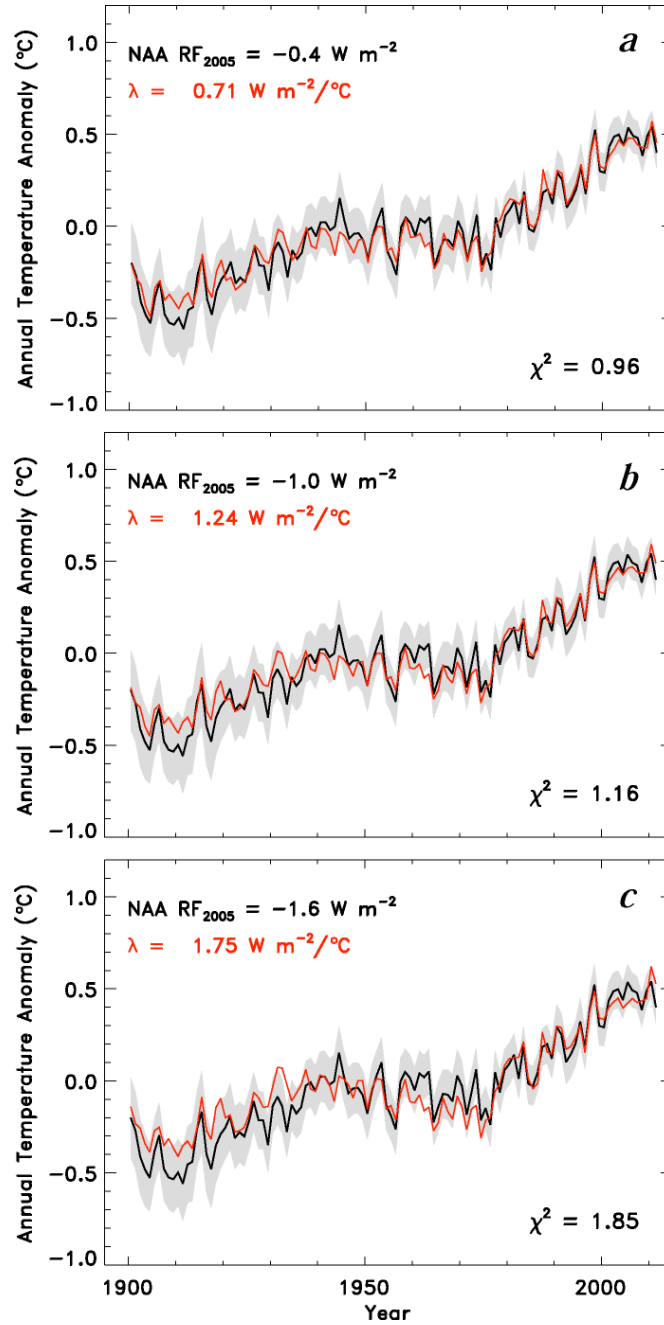


Fig. S13. Time series of the annual global mean temperature anomaly $\overline{\Delta T}_{\text{OBS}}$ (black line) and the $2 \times \overline{\sigma}_{\text{OBS}}$ uncertainty (grey shaded) from CRU4 compared to best fit simulations of the annual global mean anomaly $\overline{\Delta T}_{\text{MDL}}$ (red line) for which NAA RF_{2005} has been set to -0.4 W m^{-2} , -1.0 W m^{-2} , and -1.6 W m^{-2} for the various panels, as indicated.